

出國報告(出國類別：科學技術--國外研究、考察及國際會議)

2015 年赴新加坡國立大學淡馬錫研究中心
進行風洞實驗及研究合作
出國報告書

服務機關：國立暨南國際大學

姓名職稱：林繼耀副教授

派赴國家：新加坡

出國期日：104 年 8 月 18 日至 8 月 29 日

報告日期：105 年 3 月 21 日

摘要

暨南大學電機系 2012 年與新加坡國立大學之淡馬錫研究中心簽署合作計畫合約，合作內容是機翼氣動伺服彈性的建模與控制問題。此合作計畫屬於一項由新加坡國防部資助、淡馬錫研究中心執行的整合型計畫中的一個子計畫，出差人員林繼耀副教授為此子計畫主持人，研究工作結合了暨大林副教授在非線性系統辨識與控制設計方面的專長，以及淡馬錫研究中心流體力學計算及流體實驗方面的專長及風洞實驗設備。此計畫執行至 2014 年 12 月截止，已研發出系統建模與控制設計的方法，繼前一次(2015 年 5 月)出國商討後續工作之後，此次出國是為了進行風動實驗工作，一便驗證研發成果。

目次

一、出差事由.....	1
二、出差人員.....	1
三、背景.....	1
四、目的.....	1
五、過程.....	2
六、心得與建議.....	3
七、實驗照片.....	3

附件一：會議記錄（英文）

一、出差事由

在新加坡國立大學淡馬錫研究中心的低速風洞進行機翼顫振控制實驗。

二、出差人員

林繼耀副教授【學術研究領域：飛控與導航技術、流動感應技術、非線性動態控制、錯誤檢測、系統辨識。】

三、背景

- (一) 暨南大學電學機系於 2012 年與新加坡國立大學之淡馬錫研究中心 (Temasek Laboratories at the National University of Singapore) 建立研究計畫合約，出差人員林繼耀副教授為此計畫主持人。
- (二) 暨南大學電學機系於 2014 年與新加坡國立大學之淡馬錫研究中心為促進雙方研究與合作交流簽署合作備忘錄。
- (三) 淡馬錫研究中心網址: <http://www.temasek-labs.nus.edu.sg/>

四、目的

- (一) 暨南大學電學機系與新加坡國立大學之淡馬錫研究中心 2012 年所建立的研究合作計畫題名為 Nonlinear Reduced-Order Modeling and Adaptive Control Design for Aeroservo-Elastic Systems，內容是機翼伺服氣動彈性的建模與顫振控制問題。研究工作結合了暨大林副教授在非線性系統辨識與控制設計方面的專長，以及淡馬錫研究中心計算流體力學及流體實驗方面的專長及設備。
- (二) 此合作計畫為由淡馬錫研究中心執行的一項整合型計畫中的子計畫，主計劃經費來自新加坡國防部。計畫執行至 2014 年 12 月截止，前一次(2015 年 5 月) 林副教授出國做成果報告與商討後續工作，雙方規劃與 2015 年 8 月進行風洞實驗。
- (三) 此計畫的研究工作結合了暨大林繼耀副教授在非線性系統辨識與控制設計的專長，以及淡馬錫研究中心計算流體力學(CFD)及流體實驗方面的專長及設備，目的是設計一部能即時消除機翼顫振 (wing flutter) 的飛行控制系統。計畫執行至今 2.5 年，經過合作雙方的密切溝通、資料分享、林副教授幾次赴新加坡與合作

伙伴會面商討，進行得相當順利，已研發出系統建模與控制設計的方法，並已製成實驗品。此次出國便是為了進行風洞實驗，以便驗證研發成果。

五、過程

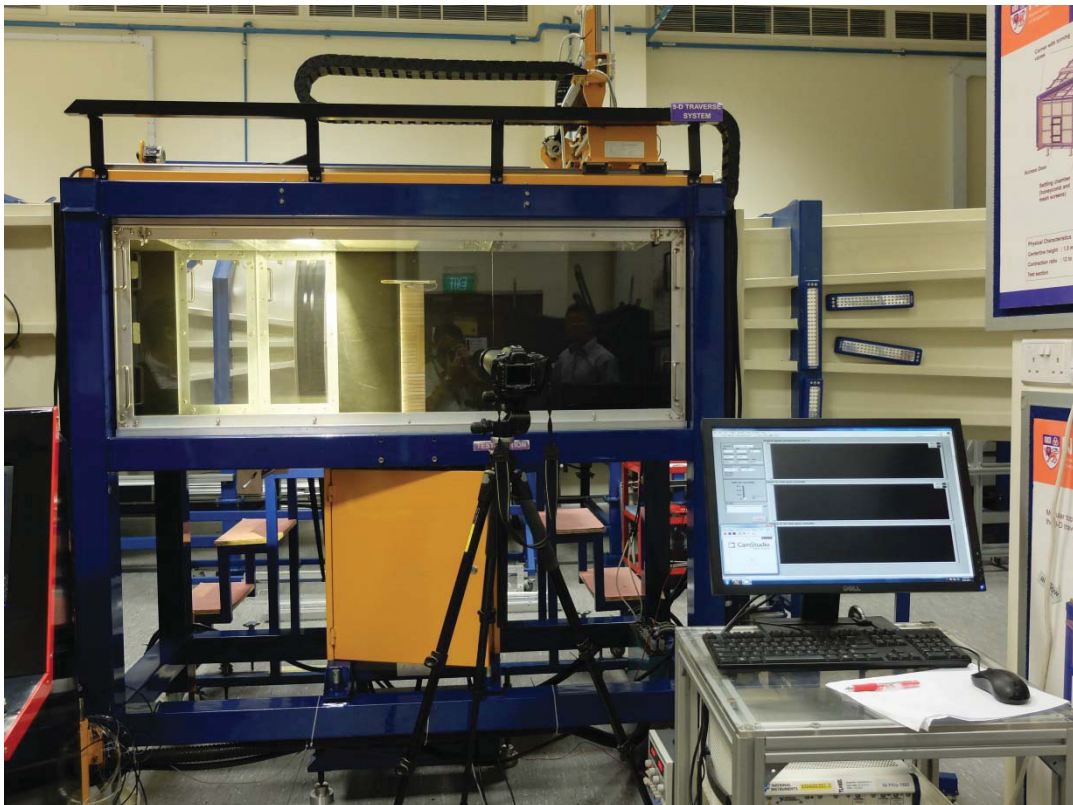
日期	地點/行程	工作記要
8/18	埔里→新加坡	啟程
8/19~8/21	新加坡，淡馬錫研究中心	出差事由：儀器校驗、實驗規劃
8/22~8/23	新加坡	個人行程(星期六、日)
8/24~8/28	新加坡，淡馬錫研究中心	出差事由：實驗進行、檢討
8/29	新加坡→埔里	回程

- (一) 實驗由暨大的林副教授主導，淡馬錫研究中心的盧鎮波博士和崔勇東博士協助進行，計畫主持人黎國樑博士監視。
- (二) 實驗場所是淡馬錫研究中心的風洞實驗室，此風洞是循環式低速風洞，於 2009 年建成，穩定風速最低可達 5m/s，最高可達 70m/s 或馬克數 0.21，為一個研究與教學設備，適合流場顯現 (flow visualization)、飛行模型的動力測試(flight model dynamic measurement)、氣動彈性與顫振(aero-elasticity and flutter)等實驗。此設備配有德州儀器數據採集裝置和 LabView 資料及控制軟體。
- (三) 第一週的工作主要是數據模型、實驗品與相關儀器的校驗，為的是確保理論與計算研究所得的數據模型複合實體模型，並確認各類儀器如傳感器、伺服馬達、濾波器等的訊號正常及其參數的設定正確。校驗過程包含以下工作：設定雜訊的濾波器、確定電位極向與傳動方向、測量顫振風速及振動頻率。
- (四) 第二週開始正式實驗，首先將控制程式實施在 LabView 中，繼而上調風速並在機翼進入顫振狀態後啟動控制程式，前後執行了有 12 個實驗，其中 3 個很顯著的驗證了在等風速及不等風速下的控制成效，成功地消除顫振。其餘實驗由於顫振狀態不強而不納入考量。
- (五) 實驗錄影：<https://youtu.be/E1rOfIXZyUo>
- (六) 最後一天小組針對實驗成果進行評估與檢討，並規劃著作發表的工作。至今有三篇論文將於今年的國際會議發表，兩篇期刊論文正在籌備中。
- (七) 其中一篇國際會議論文陳述以上實驗結果，見附件。

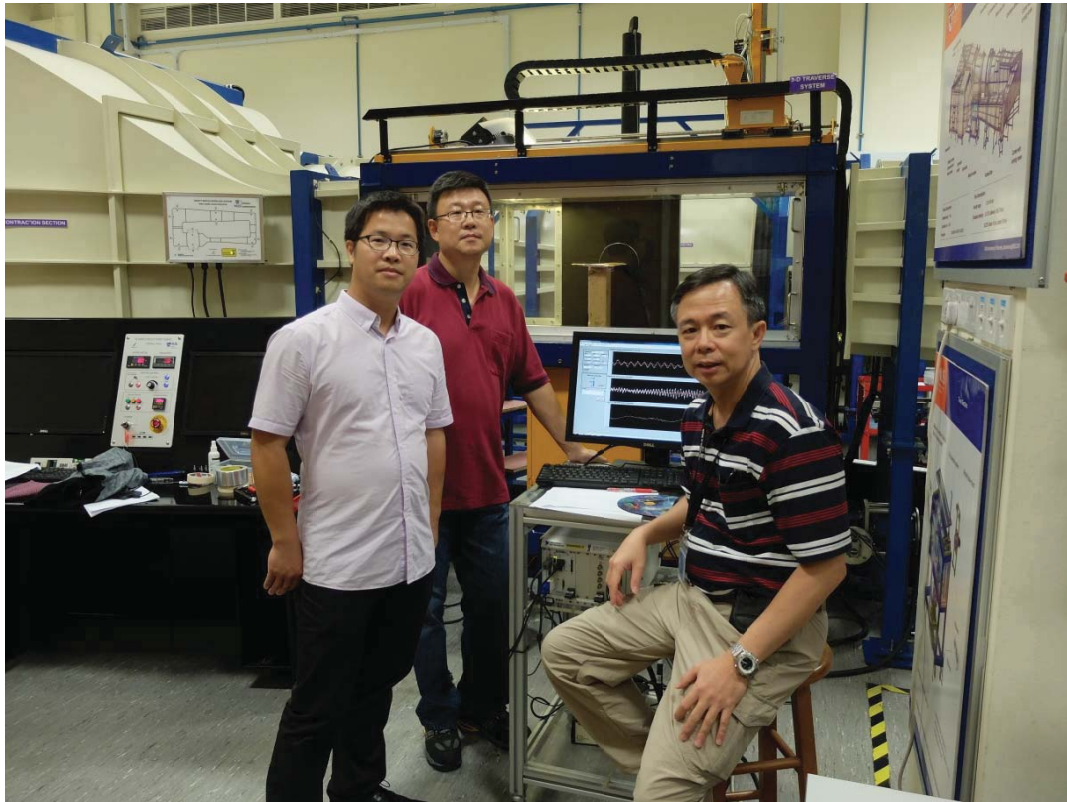
六、心得與建議

- (一) 暨大科院的規模小、資源和設備自然有限，有效的交叉領域研究需要與其他大學尤其是與外國大學建立良好的合作關係。
- (二) 此合作的基礎不僅建立在雙方的專長領域上，更重要的是雙方人員多年來的關係和友誼。(林副教授曾擔任淡馬錫中心研究員兼副主任，至 2011 年止。) 此次出國有助於計畫的圓滿完成，並有利於接下來的合作關係。
- (三) 跨國合作不只需要學術專長和經費，更需要有效的溝通，而英語為各國科技合作的共同語言，英語能力不僅在技術交流上是唯一管道，在行政上也是必備。
- (四) 要促進暨大科院各系與外國大學的合作務必讓科院課程更國際化、專科領域更深入，同時加強交叉領域的教學和研究，而且培養一個全英授課和研究的環境、加強行政人員的英語能力。

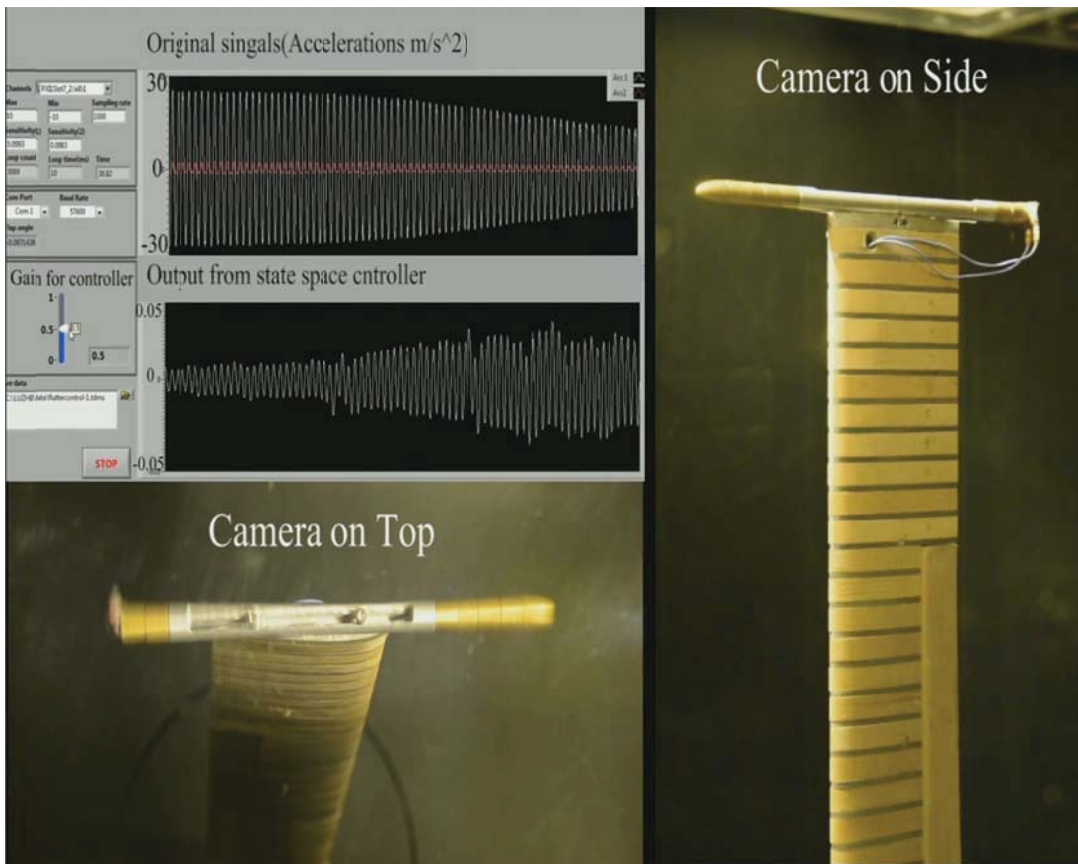
七、實驗照片



圖(一)：風洞、實驗品、儀器



圖(二)：參與人員(左至右)：盧博士、崔博士、林副教授



圖(三)：測試中

Reduced-Order Modeling and Flutter Suppression Control of an Experimental Wing*

Kai-Yew Lum^{1,3}, Cai-Lin Xu¹, Zhenbo Lu², Kwok-Leung Lai² and Yongdong Cui²

Abstract—This paper presents a numerical and experimental study of the reduced-order modeling (ROM) and flutter suppression control of a wind-tunnel wing model. The modeling work is computation based and performed in modal coordinates of the wing structure. A nonlinear ROM of aerodynamic and structural responses is obtained via computational aero-elasticity simulation, finite-element analysis and system identification. Then, casting the linearized model in linear fractional transform, a fixed-order robust controller is obtained that achieves flutter suppression over uncertain air speed.

I. INTRODUCTION

Wing flutter is caused by feedback interaction between unsteady aerodynamic forces acting on the wing, and the latter's elastic structure. Under certain flight conditions, flutter instability can result in limit-cycle oscillations (LCO) which endanger the structural integrity of the aircraft [1]. Active flutter suppression has been extensively studied; traditional approaches have employed control surfaces such flaperons as actuators [2]–[7]. In recent years, active flow control techniques have also emerged [8]–[10].

A mathematical model of aero-elastic (AE) motions is essential to model-based control design. Fig. 1 represents an AE system with control. The main modeling work centers on the aerodynamic response operator $\mathcal{F}(\cdot)$, whereas the structural response model \mathbf{P} is practically linear and well understood. First-principle equations of motion have been widely employed, wherein the aerodynamic response model is based on solutions of linearized or quasi-steady aerodynamics [2], [3], [7]. Rigid-body and 2D simplifications have also been considered [4], [5], [6].

A parallel approach is reduced-order modeling (ROM) by system identification, using experimental or flight-test data. Some works treat the AE system as a lumped model, ignoring the internal feedback structure [11], [12]. Others are based on the above first-principle models, whereby modeling errors, e.g. in the nominal aerodynamic load, are estimated via system identification [3], [13]. Meanwhile, various studies have employed high-fidelity computational aero-elasticity (CAE) simulations of the input-output data $(\mathbf{u}, v; \mathbf{y})$ to directly identify $\mathcal{F}(\cdot)$ [14]–[18].

This paper presents a numerical and experimental study of ROM and flutter suppression control of a wind-tunnel wing

*This work was supported by Temasek Laboratories at the National University of Singapore.

¹K.-Y. Lum and C.-L. Xu are with the Department of Electrical Engineering, National Chi Nan University, Taiwan 54561.

²Z. Lu, K.-L. Lai and Y. Cui are with Temasek Laboratories, National University of Singapore, Singapore 117411.

³Corresponding author. kaiyew.lum@ieee.org

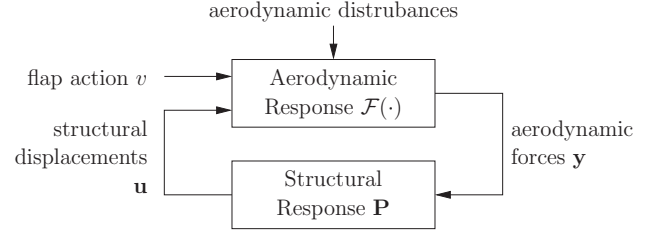


Fig. 1: Schema of an aero-elastic system

model [19]. The structural and aerodynamic response models are based on CAE data computed in the modal coordinates of a finite number of dominant modes, and system identification. The aerodynamic ROM is nonlinear, and takes a non-block form of the Hammerstein-Wiener equations with an underlying μ -Markov linear structure [20]. By linearizing the thus obtained AE system model and formulating its linear fractional transform, a fixed-order robust controller for flutter suppression under uncertain air speed is computed using the HIFOO algorithm [21]. Wind tunnel tests confirm the validity of this approach, achieving 90% attenuation of LCO.

II. REDUCED-ORDER MODELING AND IDENTIFICATION

A. Preliminary: μ -Markov Structure

The scalar μ -Markov model structure is a μ -step ahead predictor of the input-output pair (u, y) and is given by:

$$y(k) = -\sum_{j=1}^{n_a} a_j y(k-\mu+1-j) + \sum_{i=r}^{r+\mu-1} h_i u(k-i) + \sum_{i=r+1}^{n_b} b_i u(k-\mu+1-i). \quad (1)$$

In the above, μ is the number of Markov parameters in the model, n_a and n_b are the model orders, and r is the input delay. In particular, $\mu = 1$ recovers the standard ARMA structure [20], [22].

B. Hammerstein-Wiener-like Model with μ -Markov Structures

Consider now a nonlinear, multiple-input multiple-output (MIMO) extension of (1) given by

$$\begin{aligned} \mathbf{y}(k) = & -z^{-\mu+1}(\mathbf{A}(z^{-1}) \circ \bar{\alpha}[\cdot])\mathbf{y}(k) \\ & + z^{-r}(\mathbf{H}(z^{-1}) \circ \bar{\gamma}[\cdot])\mathbf{u}(k) + z^{-r}(\mathbf{h}(z^{-1}) \circ \bar{\beta}[\cdot])v(k) \\ & + z^{-(r+\mu)}(\mathbf{B}(z^{-1}) \circ \bar{\gamma}[\cdot])\mathbf{u}(k) + z^{-(r+\mu)}(\mathbf{b}(z^{-1}) \circ \bar{\beta}[\cdot])v(k), \end{aligned} \quad (2)$$

where $\mathbf{y} = [y_1, \dots, y_N]^T$, $\mathbf{u} = [u_1, \dots, u_N]^T$, and z^{-1} denotes the delay operator. \mathbf{A} , \mathbf{H} and \mathbf{B} are $N \times N$ transfer-function

matrices, whereas \mathbf{h} and \mathbf{b} are $N \times 1$; they are further expressed in terms of their elements as:

$$\begin{aligned} \mathbf{A}(z^{-1}) &= [A_{ij}(z^{-1})]_{i,j=1,\dots,N}, \\ \mathbf{H}(z^{-1}) &= [H_{ij}(z^{-1})]_{i,j=1,\dots,N}, \quad \mathbf{h}(z^{-1}) = [h_i(z^{-1})]_{i=1,\dots,N}, \\ \mathbf{B}(z^{-1}) &= [B_{ij}(z^{-1})]_{i,j=1,\dots,N}, \quad \mathbf{b}(z^{-1}) = [b_i(z^{-1})]_{i=1,\dots,N}, \end{aligned}$$

with the following scalar transfer functions:

$$\begin{aligned} A_{ij}(z^{-1}) &= A_{ij}^{(1)} z^{-1} + \dots + A_{ij}^{(n_a)} z^{-\mu+1}, \\ H_{ij}(z^{-1}) &= H_{ij}^{(0)} + H_{ij}^{(1)} z^{-1} + \dots + H_{ij}^{(\mu-1)} z^{-\mu+1}, \\ h_i(z^{-1}) &= h_i^{(0)} + h_i^{(1)} z^{-1} + \dots + h_i^{(\mu-1)} z^{-\mu+1}, \\ B_{ij}(z^{-1}) &= B_{ij}^{(0)} + B_{ij}^{(1)} z^{-1} + \dots + B_{ij}^{(n_b)} z^{-\mu+1}, \\ b_i(z^{-1}) &= b_i^{(0)} + b_i^{(1)} z^{-1} + \dots + b_i^{(n_b)} z^{-\mu+1}. \end{aligned}$$

Furthermore, the operators $\bar{\alpha}[\cdot]$ and $\bar{\gamma}[\cdot]$ represent $N \times N$ matrices of polynomial functions, whereas $\bar{\beta}[\cdot]$ is $N \times 1$; they are defined as follows:

$$\begin{aligned} \bar{\alpha}[\cdot] &= [\bar{\alpha}_{ij}(\cdot)]_{i,j=1,\dots,N}, \quad \bar{\alpha}_{ij}(\nu) = \sum_{l=1}^q \alpha_{ij}^{[l]} \nu^l, \quad \nu \in \mathbb{R}, \\ \bar{\gamma}[\cdot] &= [\bar{\gamma}_{ij}(\cdot)]_{i,j=1,\dots,N}, \quad \bar{\gamma}_{ij}(\nu) = \sum_{l=1}^p \gamma_{ij}^{[l]} \nu^l, \quad \nu \in \mathbb{R}, \\ \bar{\beta}[\cdot] &= [\bar{\beta}_i(\cdot)]_{i=1,\dots,N}, \quad \bar{\beta}_i(\nu) = \sum_{l=1}^p \beta_i^{[l]} \nu^l, \quad \nu \in \mathbb{R}, \end{aligned}$$

where $\alpha_{ij}^{[l]}$, $\gamma_{ij}^{[l]}$, $\beta_i^{[l]}$ are scalar coefficients, and p and q are some fixed positive integers. Finally, “ \circ ” in (2) denotes the Hadamard product of the respective operators. Thus, expanding (2) yields the following equation for each mode y_i , $i = 1, \dots, N$:

$$\begin{aligned} y_i(k) &= -z^{-\mu+1} \sum_{j=1}^N \sum_{l=1}^q A_{ij}(z^{-1}) \alpha_{ij}^{[l]} y_j^l(k) \\ &+ z^{-r} \left\{ \sum_{j=1}^N \sum_{l=1}^p H_{ij}(z^{-1}) \gamma_{ij}^{[l]} u_j^l(k) + \sum_{l=1}^p h_i(z^{-1}) \beta_i^{[l]} v^l(k) \right\} \\ &+ z^{-(r+\mu)} \left\{ \sum_{j=1}^N \sum_{l=1}^p B_{ij}(z^{-1}) \gamma_{ij}^{[l]} u_j^l(k) + \sum_{l=1}^p b_i(z^{-1}) \beta_i^{[l]} v^l(k) \right\}. \end{aligned} \quad (3)$$

Remark 1: The nonlinear model (2) or, equivalently, (3) is unlike the classical Hammerstein-Wiener model, as it is evident that the Hadamard product in (2) does not allow separation into a block-oriented form. Thus the name *Hammerstein-Wiener-like* (HWL). Fig. 2 gives a block diagram.

C. Identification of HWL ROM for Aerodynamic Response

Based on the aforementioned HWL model (3), a ROM of the aerodynamic response operator $\mathcal{F}(\cdot)$ can be represented as

$$\mathcal{F}(\cdot) \sim_N \{ \mathbf{A}, \mathbf{H}, \mathbf{h}, \mathbf{B}, \mathbf{b}, \bar{\alpha}, \bar{\beta}, \bar{\gamma} \} \quad (4)$$

where the symbol \sim with subscript N signifies an N -modal ROM; the right-hand side of (4) is defined for some

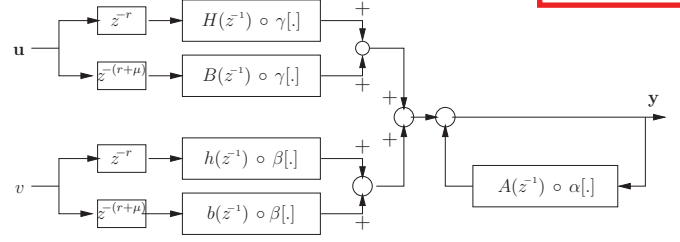


Fig. 2: Hammerstein-Wiener-like model

chosen model orders (μ, n_a, n_b, r, p, q) . In modal coordinates, N is the number of dominant modes to be considered, thus ignoring higher-order aero-elasticity. Modeling thus consists in identifying the parameters $A_{ij}^{(k)}$, $H_{ij}^{(0)}$, $h_i^{(k)}$, $B_{ij}^{(k)}$, $b_i^{(k)}$, $\alpha_{ij}^{[l]}$, $\beta_i^{[l]}$ and $\gamma_{ij}^{[l]}$. A total of $N^2(n_a + 2\mu + 2(n_b + 1)) + 2N\mu + N^2(q + 2p)$ parameters will need to be identified.

The proposed HWL model can be viewed as a MIMO extension of a nonlinear model with ARMA structure considered in [23], wherein a two-stage algorithm based on singular-value decomposition was given for the identification of SISO models. Here, this method is extended to the MIMO model (3). Details are omitted.

Parameter identification is performed using input-output data generated in open-loop CFD simulation. In other words, the input \mathbf{u} are prescribed functions of time acting as modal displacements, and the generalized aerodynamic forces \mathbf{y} as response to those displacements are solutions of a full-order flow solver [24].

III. ROBUST FLUTTER SUPPRESSION CONTROL

Design of flutter suppression control is performed on a linearized model of the aero-elastic system shown in Fig. 3. Linearization concerns two aspects: first, the aerodynamic ROM $\mathcal{F}(\cdot)$ defined in (4) is linearized about zero modal displacements and forces; second, the structural response operator \mathbf{P} in Fig. 1 is replaced by a finite-order linear system. Robust control design is then performed for an uncertain speed index V . Details follow.

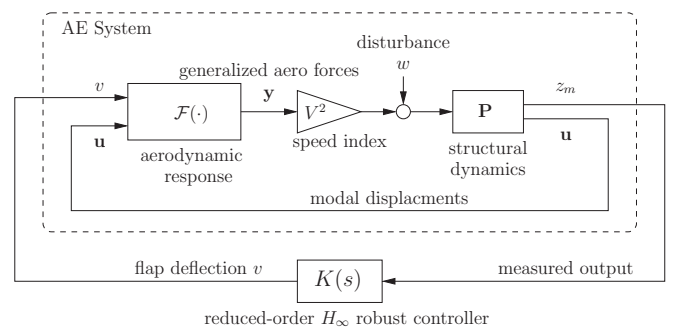


Fig. 3: Flutter suppression control block diagram

Remark 2: Even though control design is based on the linearized AE system, it is important to note that system identification of a nonlinear ROM for $\mathcal{F}(\cdot)$ is necessary, as a linear model would yield poor estimates of the poles and zeros [20].

A. State-Space Model of Linear AE System

1) *Linearized aerodynamic ROM*: Linearization of the HWL model (2) at zero \mathbf{u} and \mathbf{y} retains only the $N \times N$ μ -Markov system $\{A, \mathbf{H}, \mathbf{h}, B, \mathbf{b}\}$, of which a discrete-time state-space realization can be computed using the eigenrealization algorithm [25]. Furthermore, by Tustin's transform, a continuous-time state-space model Σ_f of linearized aerodynamics can be obtained. Let Σ_f be represented by:

$$\mathcal{F}(\cdot) \stackrel{\text{linear}}{\sim}_N \Sigma_f: \begin{cases} \dot{x}_f = A_f x_f + B_f \mathbf{u} + b_f v, \\ \mathbf{y} = C_f x_f + D_f \mathbf{u} + d_f v, \end{cases} \quad (5)$$

where $x_f \in \mathbb{R}^{n_f}$ are the internal states of dimension n_f depending on the ROM.

2) *Modal equations of structural dynamics*: In modal coordinates, each mode of the structural dynamics is described by a linear second-order system:

$$\ddot{u}_i + 2\zeta_i \omega_i \dot{u}_i + \omega_i^2 u_i = \alpha V^2 y_i, \quad (6)$$

where ζ_i and ω_i are the associated damping factor and natural frequency, α is a flow condition-dependent constant, and V is a non-dimensional quantity related to airspeed [24], [26]. For the first N dominant modes, i.e. with $i = 1, \dots, N$, a state-space representation Σ_s of linear structural dynamics is thus given by:

$$\mathbf{P} \stackrel{\sim}{\sim}_N \Sigma_s: \begin{cases} \dot{x}_s = A_s x_s + B_s (V^2 \mathbf{y} + w), \\ \mathbf{u} = C_s x_s, \\ z_m = H_s x_s, \end{cases} \quad (7)$$

where the system matrices are

$$A_s = \text{diag}[A_s^1 \ \dots \ A_s^N], \quad B_s = \text{diag}[B_s^1 \ \dots \ B_s^N], \\ A_s^i = \begin{bmatrix} 0 & 1 \\ -\omega_i^2 & -2\zeta_i \omega_i \end{bmatrix}, \quad B_s^i = \begin{bmatrix} 0 \\ \alpha \end{bmatrix},$$

C_s is straight-forward, and w is an assumed disturbance. In the above, z_m represents a physically measured output of the AE system, e.g. acceleration picked up by sensors. The rows of the output matrix H_s are thus the sensor locations in modal coordinates, and are computed using finite-element analysis (FEA).

3) *AE closed-loop model*: Based on (5) and (7), the AE system in feedback of Fig. 3 is represented by the following closed-loop equations:

$$\begin{bmatrix} \dot{x}_s \\ \dot{x}_f \end{bmatrix} = \begin{bmatrix} A_s + V^2 B_s D_f C_s & V^2 B_s C_f \\ B_f C_s & A_f \end{bmatrix} \begin{bmatrix} x_s \\ x_f \end{bmatrix} \\ + \begin{bmatrix} B_s \\ 0 \end{bmatrix} w + \begin{bmatrix} V^2 B_s d_f \\ b_f \end{bmatrix} v, \quad (8a)$$

$$z_m = [H_s \ 0] \begin{bmatrix} x_s \\ x_f \end{bmatrix}, \quad (8b)$$

which takes the form:

$$\Sigma_{\text{AE}}: \begin{cases} \dot{x} = \hat{A}x + \hat{B}_1 w + \hat{B}_2 v, & x = (x_s, x_f) \\ z_m = C_2 x. \end{cases} \quad (9)$$

B. Uncertainty Model and Linear Fractional Transform

By Hopf bifurcation analysis, the onset of flutter corresponds to the crossing of the imaginary axis by a pair of

eigenvalues of Σ_{AE} as the speed index increases past a cross-over value V_f [14], [18]. To achieve flutter suppression, the control objective is to stabilize Σ_{AE} for uncertain speed index near V_f . In other words, stability is to be guaranteed for

$$V^2 = V_f^2 + \Delta V, \quad \Delta V < \frac{1}{\gamma}, \quad (10)$$

where $\Delta V \triangleq V^2 - V_f^2$, and γ is desired to be small so that the stability range is large. Flutter suppression is thus a robust stability margin problem [3].

Substituting (10) into (8) and (9), one obtains the following uncertainty expressions:

$$\hat{A} = A + \Delta A, \quad \hat{B}_1 = B_1 + \Delta B_1, \quad \hat{B}_2 = B_2 + \Delta B_2 \quad (11a)$$

with

$$A = \begin{bmatrix} A_s + V_f^2 B_s D_f C_s & V_f^2 B_s C_f \\ B_f C_s & A_f \end{bmatrix}, \quad (11b)$$

$$\Delta A = \begin{bmatrix} \Delta V B_s D_f C_s & \Delta V B_s C_f \\ 0 & 0 \end{bmatrix}, \quad (11c)$$

$$B_1 = \begin{bmatrix} B_s \\ 0 \end{bmatrix}, \quad \Delta B_1 = \begin{bmatrix} 0 \\ 0 \end{bmatrix}, \quad (11d)$$

$$B_2 = \begin{bmatrix} V_f^2 B_s d_f \\ b_f \end{bmatrix}, \quad \Delta B_2 = \begin{bmatrix} \Delta V B_s d_f \\ 0 \end{bmatrix}. \quad (11e)$$

The following lemmas are straight-forward.

Lemma 1: The uncertainty matrices ΔA , ΔB_1 and ΔB_2 can be decomposed into the form:

$$[\Delta A \ \Delta B_1 \ \Delta B_2] = -M_x \Delta V [N_x \ N_w \ N_v], \quad (12)$$

where

$$M_x = \begin{bmatrix} -B_s \\ 0 \end{bmatrix}, \quad N_x = [D_f C_s \ C_f], \quad N_w = 0, \quad N_v = d_f.$$

Lemma 2: Define the fictitious input w_f and output z_f :

$$z_f = [N_x \ 0 \ N_w \ N_v] \begin{bmatrix} x \\ w_f \\ w \\ v \end{bmatrix}. \quad (13)$$

Then the AE system Σ_{AE} (9) with uncertainties (11a) can be expressed as the following linear fractional transform (LFT) with internal feedback (see Fig. 4):

$$\begin{bmatrix} \dot{x} \\ z_f \\ z_m \end{bmatrix} = \begin{bmatrix} A & \bar{B}_1 & B_2 \\ \hline C_1 & D_{11} & D_{12} \\ C_2 & 0 & 0 \end{bmatrix} \begin{bmatrix} x \\ \bar{w} \\ v \end{bmatrix}, \quad (14)$$

where

$$\bar{w} = \begin{bmatrix} w_f \\ w \end{bmatrix}, \quad \bar{B}_1 = [M_x \ B_1],$$

$$C_1 = N_x, \quad D_{11} = [0 \ N_w], \quad D_{12} = \begin{bmatrix} N_v \\ D_{12} \end{bmatrix},$$

and the internal feedback is given by

$$w_f = -\Delta V z_f. \quad (15)$$

C. Fixed-Order Robust Control

The problem of flutter suppression translates into finding a robust output-feedback controller $K(s)$ for the LFT system

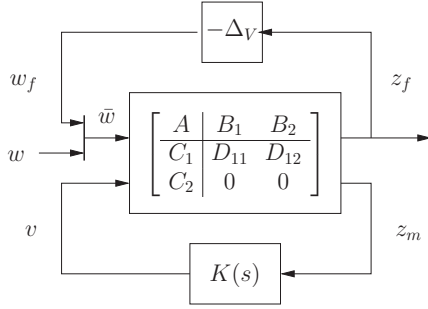


Fig. 4: LFT system with internal feedback and output-feedback control

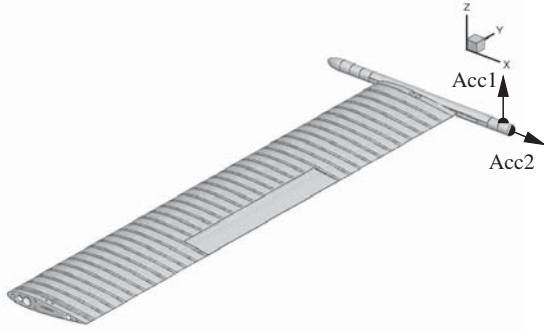


Fig. 5: Experimental wing with sensor placement. Acc1: bending and torsional accelerometer; Acc2: lateral accelerometer.

(14) that minimizes its H_∞ norm $\|T_{\bar{w}z_f}\|_\infty$. A sufficient condition is that $K(s)$ stabilizes the nominal system and satisfies

$$\|T_{\bar{w}z_f}\|_\infty < \gamma \quad (16)$$

for some γ small enough; by the small gain theorem, the stability of the closed loop is guaranteed for all perturbations satisfying $|\Delta_V| < \frac{1}{\gamma}$ [27].

The standard H_∞ output-feedback full-order controller is not practical for the AE system given the latter's high-order (25th; see later). On the other hand, reduced-order H_∞ controller design is a difficult non-convex optimization problem. To overcome the latter, this work seeks a fixed-order H_∞ controller by means of a non-convex local optimization algorithm that offers the advantage of stability guarantee when a solution is found, and handling of non-smooth gradients encountered in non-convex problems [21], [28].

IV. NUMERICAL AND EXPERIMENTAL RESULTS

The proposed approach is applied to an experimental wing and tested in a low-speed wind-tunnel (Fig. 5). The wing has been specially designed so that flutter occurs with sustained LCO at a relatively low speed, between 20m/s and 40m/s. A beam-like wing with tip store has been adopted as it fits these requirements [19]. FEA reveals five dominant modes as shown in Fig. 6 with their modal frequencies. Table I lists the key parameters.

TABLE I: Key parameters

nominal speed index	$V_o = 0.69$
nominal air speed	20 m/s
nominal Mach number	0.06
number of modes	$N = 5$
(μ, n_a, n_b, r, p, q)	$(3, 1, 1, 1, 2, 2)$
order of Σ_f	$n_f = 15$
order of Σ_s	10
order of Σ_{AE}	25
flutter speed index*	$V_f = 1.20$
flutter air speed*	34.7 m/s
order of controller $K(s)$	3
number of sensors	$\dim(z_m) = 2$

* flutter speeds are determined numerically

Two accelerometers are attached to the tip store, of which the first is predominantly sensitive to the bending and torsional modes, and the second to the lateral mode. This is evident in the sensor locations in modal coordinates:

$$\begin{bmatrix} 0.1299 & -0.0006 & -0.2866 & -0.1130 & 0.0766 \\ -0.0021 & 0.1364 & 0.0141 & 0.0021 & -0.0020 \end{bmatrix}.$$

A. Model Identification & Validation

1) *System identification*: A full-order CAE simulation of the wing has been conducted with prescribed modal displacements in the form of band-limited chirp signals [20], at the nominal speed and Mach number. As a result of this the first five modal displacements and generalized aerodynamic forces are used for the identification of a HWL ROM. Fig. 7 shows that there is a good fit between ROM and CAE responses, with less than 1% error in all except the 2nd mode which exhibits pronounced nonlinear behavior.

2) *Model validation against experiment*: A key concern in this study is the fidelity of the CAE and FEA solutions and, consequently, the validity of the aerodynamic ROM and structural dynamics model. To ascertain this, simulations of the nonlinear AE system, i.e. ROM $\mathcal{F}(\cdot)$ in feedback interaction with the finite-order structural model Σ_s , are conducted and the responses compared with accelerometer measurements obtained in experiment. Fig. 8 shows the

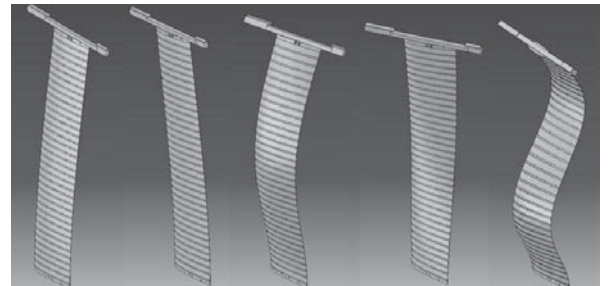


Fig. 6: Wing modal shapes and frequencies obtained in FEA (left to right): 1st bending (2.19Hz), 1st lateral (10.07Hz), 2nd bending (13.55Hz), 1st torsional (16.48Hz), 3rd bending (38.09Hz).

simulated and measured responses of the first sensor for a given sequence of flap angle commands (in fact, a finite-width impulse response of the controller). After adjusting for sensor bias and filtering noise, it can be seen that the simulated response closely resembles the measurement.

A second validation is done by first performing Hopf bifurcation analysis of the ROM, which yields a flutter speed index of $V_f = 1.20$, i.e. at which a pair of eigenvalues of Σ_{AE} crosses the imaginary axis. Next, nonlinear ROM simulation at this speed produces LCO (instead of divergence) as shown in the bottom graph of Fig. 9. Moreover, the top graph shows a good agreement between the spectrum of the simulated LCO and that measured in the wind tunnel at the same speed. In particular, both reveal a fundamental LCO frequency of $\omega_f = 8.5$ Hz.

B. Control Design & Linear Analysis

A third-order controller has been found that stabilizes the linear AE system Σ_{AE} for $V \in (0, 2.4)$. Fig. 10 shows the pole loci of both the open- and closed-loop linear AE system. It can be seen that at the open-loop flutter speed index $V_f = 1.20$, the closed-loop system's poles remain on the left-hand plane, whereas for the open-loop system the pair of poles evolving from the 2nd mode (lateral) crosses the imaginary axis.

C. Wind Tunnel Experiment

Finally, flutter suppression control experiments are conducted in the wind tunnel. Fig. 11 shows a screen shot of the experiment and real-time recording, as well as the time history of sensor measurements during one run. In order to avoid abrupt action by the flap, a gain factor is applied to the controller and increased slowly from zero to 1. It can be that when the gain factor exceeds 1, flutter is suppressed by more than 90%. On the release of the controller, flutter reappears, which fully validates the control performance. A video of the experiment can be viewed at <https://youtu.be/E1rOfIXZyUo>.

V. CONCLUDING REMARKS

This study has demonstrated the feasibility of the proposed ROM approach. In particular, model fidelity has been experimentally confirmed, which lends confidence to control design. Robust control over air-speed uncertainty effectively achieves flutter suppression.

This work is focused on stabilization of the LFT model (14) using HIFOO-based control design, whereas performance is a secondary concern. Meanwhile, the observability of (14) is important as it concerns sensor placement; an analysis thereof will be addressed in a future publication.

It is worth noting that the present study only considers the wing in a vertical position with zero angle of attack, i.e. its reference state is non-loaded. An extension can be envisaged to address aerodynamic load and gravity at different angles of attack. More crucially, the present formulation does not account for a varying angle of attack and dynamic pressure. Future work should consider LPV methods, adaptive control and robustness to changing flight conditions.

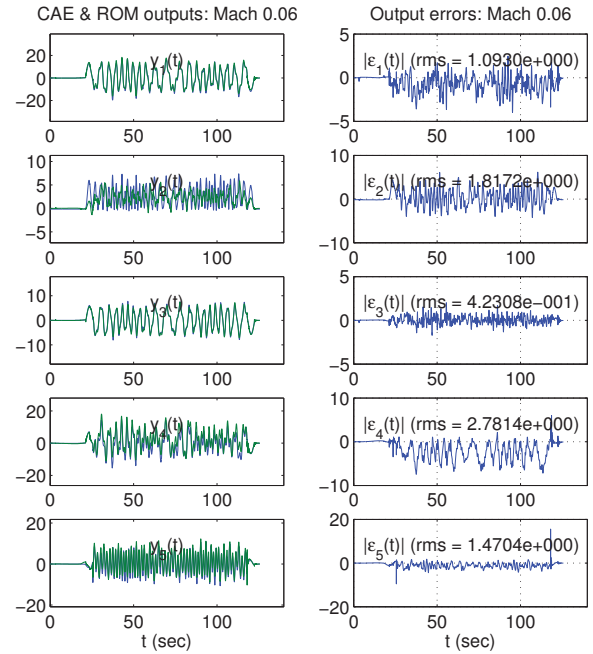


Fig. 7: System identification: goodness of fit

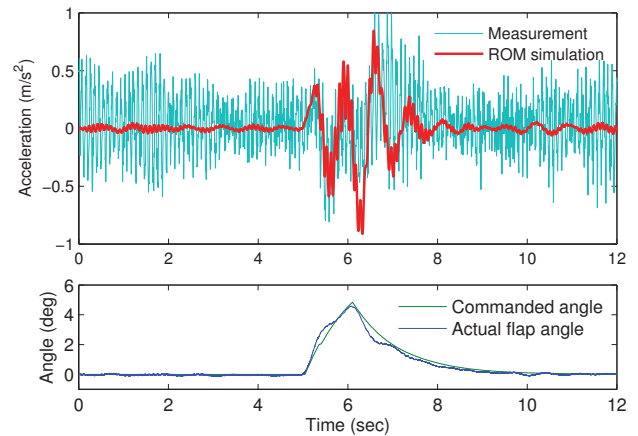


Fig. 8: Model validation

REFERENCES

- [1] J. R. Wright and J. E. Cooper, *Introduction to Aircraft Aeroelasticity and Loads*, 2nd ed. U.K.: Wiley, 2014.
- [2] J. W. Edwards, J. V. Breakwell, and A. E. Bryson Jr., "Active flutter control using generalized unsteady aerodynamic theory," *J. Guidance, Control, and Dynamics*, vol. 1, no. 1, pp. 32–40, 1978.
- [3] R. Lind and M. J. Brenner, "Robust flutter margin analysis that incorporates flight data," NASA Dryden Flight Research Center, Edwards, CA, Tech. Rep., 1998.
- [4] M. R. Waszak, "Robust multivariable flutter suppression for benchmark active controls technology wind-tunnel model," *J. Guidance, Control, and Dynamics*, vol. 24, no. 1, pp. 147–153, 2001.
- [5] P. Marzocca, L. Librescu, and W. A. Silva, "Flutter, postflutter, and control of a supersonic wing section," *J. Guidance, Control, and Dynamics*, vol. 25, no. 5, pp. 962–970, Sept. 2002.
- [6] K. Zhang, Z. Wang, A. Behal, and P. Marzocca, "Novel nonlinear control design for a two-dimensional airfoil under unsteady flow," *J. Guidance, Control, and Dynamics*, vol. 36, no. 6, pp. 1681–1694, 2013.
- [7] K. W. Lee and S. N. Singh, "Adaptive control of multi-input aeroelastic system with constrained inputs," *J. Guidance, Control, and Dynamics*, pp. 1–14, 2015.
- [8] K. Palaniappan, P. Sahu, A. Jameson, and J. J. Alonso, "Design of

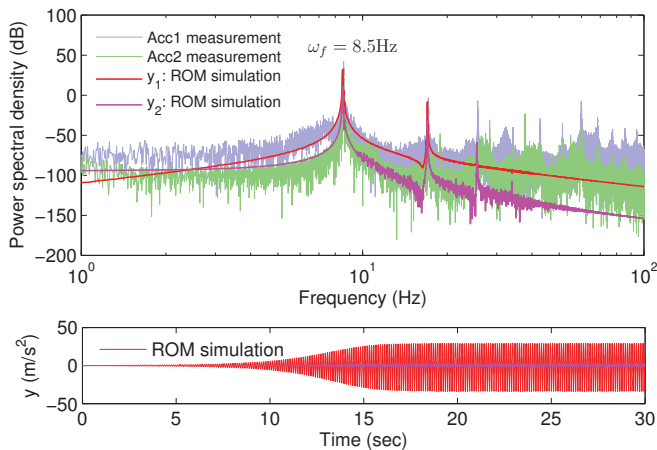


Fig. 9: Top: measured and ROM-simulated power spectral densities of LCO at $V_f = 1.20$; agreement in fundamental frequency: $\omega_f = 8.5\text{Hz}$. Bottom: ROM-simulated LCO.

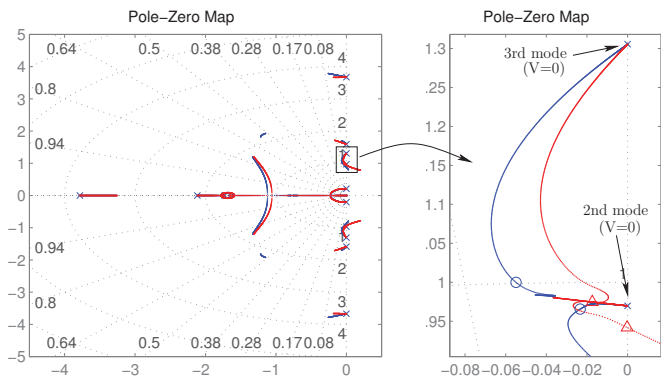


Fig. 10: Pole loci as functions of speed index: — without control, Δ poles at $V_f = 1.20$; — with control, \circ poles at $V_f = 1.20$.

adjoint-based laws for wing flutter control,” *J. Aircraft*, vol. 48, no. 1, pp. 331–335, 2011.

[9] J. Seidel, C. P. Fagley, and T. E. McLaughlin, “Computations of active open-loop flow control on a fluttering wing,” in *33rd AIAA Applied Aerodynamics Conference*. American Institute of Aeronautics and Astronautics, 2015.

[10] Z. Zhang, P. C. Chen, S. Yang, Z. Wang, and Q. Wang, “Unsteady aerostructure coupled adjoint method for flutter suppression,” *AIAA Journal*, vol. 53, no. 8, pp. 2121–2129, 2015.

[11] E. Feron, M. Brenner, and J. Paduano, “Time-frequency analysis for transfer function estimation and application to flutter clearance,” *J. Guidance, Control, and Dynamics*, vol. 21, no. 3, pp. 375–382, 1998.

[12] D. Baldelli, J. Zeng, R. Lind, and C. Harris, “Robust flutter prediction for data-based aeroelastic LPV models,” in *Proc. AIAA Atmospheric Flight Mechanics Conference and Exhibit*, Hilton Head, SC, USA, Aug. 20–23 2007, pp. AIAA Paper 2007–6301.

[13] D. H. Baldelli, R. Lind, and M. Brenner, “Control-oriented flutter/limit-cycle-oscillation prediction framework,” *J. Guidance, Control, and Dynamics*, vol. 31, no. 6, pp. 1634–1643, 2008.

[14] P. Beran and W. Silva, “Reduced-order modelling: new approaches for computational physics,” in *Proc. 39th Aerospace Sciences Meeting*, Reno, NV, USA, Jan. 8–11 2001.

[15] T. Cowan, A. Arena, and K. Gupta, “Accelerating computational fluid dynamics based aeroelastic predictions using system identification,” *J. Aircraft*, vol. 38, no. 1, pp. 81–87, 2001.

[16] W. Silva, “Identification of nonlinear aeroelastic systems based on the Volterra theory: Progress and opportunities,” *Nonlinear Dynamics*, vol. 39, no. 1–2, pp. 25–62, 2005.

[17] M. Balajewicz and E. Dowell, “Reduced-order modeling of flutter and limit-cycle oscillations using the sparse volterra series,” *J. Aircraft*,

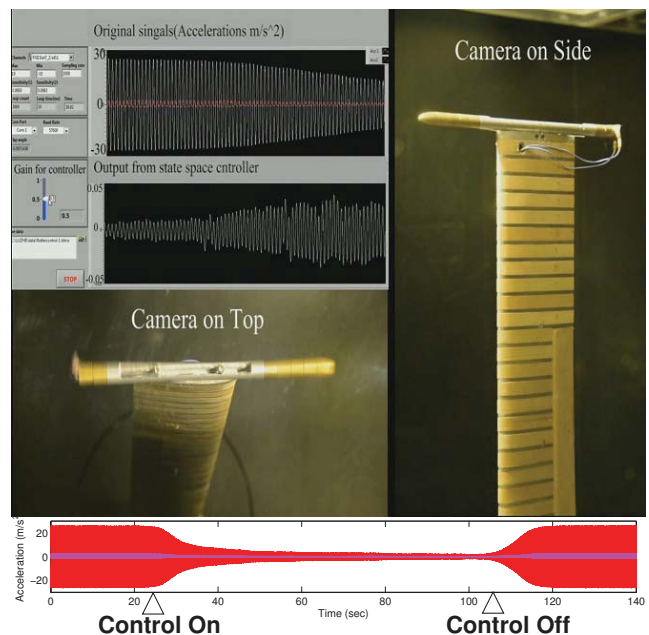


Fig. 11: Top: screen shot of wind tunnel experiment. Bottom: time history of sensor measurements. Video: <https://youtu.be/E1rOfiXZyUo>

vol. 49, no. 6, pp. 1803–1812, Nov. 2012.

[18] K.-Y. Lum and K.-L. Lai, “Reduced order flutter modeling based on the Hammerstein model with μ -Markov structure and correlation identification method,” in *2014 SICE Annual Conference*, Sapporo, Japan, Sept 2014.

[19] Z. Lu, Y. Cui, D. J. Schneider, Z. Zhao, X. Chen, K. L. Lai, and K.-Y. Lum, “Aeroelastic responses identification of a high-aspect-ratio flexible wing model and its active flutter suppression strategy,” in *57th AIAA/ASCE/AHS/ASC Structures, Structural Dynamics, and Materials Conference*, San Diego, CA, Jan 4–8 2016.

[20] K.-Y. Lum and D. S. Bernstein, “A correlation least-squares method for Hammerstein model identification with ARX and μ -Markov structures,” in *IFAC World Congress*, vol. 18, Milano, 2011, pp. 11 183–9.

[21] J. V. Burke, H. D., A. S. Lewis, and M. L. Overton, “HIFOO - a MATLAB package for fixed-order controller design and H_∞ optimization,” in *IFAC Symposium on Robust Control Design*, Toulouse, Jul. 5–7 2006.

[22] R. Venugopal and D. Bernstein, “Adaptive disturbance rejection using ARMARKOV/Toeplitz models,” *IEEE Trans. on Control Systems Technology*, vol. 8, no. 2, pp. 257–269, March 2000.

[23] E.-W. Bai, “An optimal two stage identification algorithm for Hammerstein-Wiener nonlinear systems,” *Proc. of the American Control Conference*, 1998.

[24] K. L. Lai, L. Carolina, and H. Tsai, “Aeroelastic simulations using gridless boundary condition and small perturbation techniques,” *Computers & Fluids*, vol. 39, pp. 829–844, 2010.

[25] J. N. Juang and R. S. Appa, “An eigensystem realization algorithm for modal parameter identification and model reduction,” *J. Guidance, Control, and Dynamics*, vol. 8, no. 5, pp. 620–627, 1985.

[26] P. Leyland, F. Blom, V. Carstens, and T. Tefy, “Fully coupled fluid-structure algorithms for aeroelasticity and forced vibration induced flutter: Applications to a compressor cascade,” in *Fluid-Structure Interaction*. Kogan Page Science, 2003, pp. 137–178.

[27] K. Zhou and J. C. Doyle, *Essentials of Robust Control*. NJ: Prentice Hall, 1998.

[28] J. Burke, D. Henrion, A. Lewis, and M. Overton, “Stabilization via nonsmooth, nonconvex optimization,” *IEEE Trans. on Automatic Control*, vol. 51, no. 11, pp. 1760–1769, Nov 2006.